JACS
JOURNAL OF THE AMERICAN CHEMICAL SOCIETY

ARTICLE

pubs.acs.org/JACS

Periodic Mesoporous Hydridosilica — Synthesis of an "Impossible" Material and Its Thermal Transformation into Brightly Photoluminescent Periodic Mesoporous Nanocrystal Silicon-Silica Composite

Zhuoying Xie,[†,‡] Eric J. Henderson,[†] Ömer Dag,[§] Wendong Wang,[†] Jennifer E. Lofgreen,[†] Christian Kübel,[∥,⊥] Torsten Scherer,[∥,⊥] Peter M. Brodersen,[#] Zhong-Ze Gu,[*,‡] and Geoffrey A. Ozin[*,†]

[†]Materials Chemistry and Nanochemistry Research Group, Center for Inorganic and Polymeric Nanomaterials, Chemistry Department, 80 St. George Street, University of Toronto, Toronto, Ontario, Canada M5S 3H6

[‡]State Key Laboratory of Bioelectronics, Southeast University, Nanjing, P. R. China 210096

[§]Department of Chemistry, Bilkent University, 06800 Ankara, Turkey

[∥]Karlsruhe Institute of Technology, Institute of Nanotechnology, Eggenstein-Leopoldshafen, Germany

[⊥]Karlsruhe Nano Micro Facility, Eggenstein-Leopoldshafen, Germany

[#]Surface Interface Ontario (SIO), University of Toronto, Toronto, Ontario, Canada M5S 3E5

Supporting Information

ABSTRACT: There has always been a fascination with "impossible" compounds, ones that do not break any rules of chemical bonding or valence but whose structures are unstable and do not exist. This instability can usually be rationalized in terms of chemical or physical restrictions associated with valence electron shells, multiple bonding, oxidation states, catenation, and the inert pair effect. In the pursuit of these "impossible" materials, appropriate conditions have sometimes been found to overcome these instabilities and synthesize missing compounds, yet for others these tricks have yet to be uncovered and the materials remain elusive. In the scientifically and technologically important field of periodic mesoporous silicas (PMS), one such "impossible" material is periodic mesoporous hydridosilica (meso-$HSiO_{1.5}$). It is the archetype of a completely interrupted silica open framework material: its pore walls are comprised of a three-connected three-dimensional network that should be so thermodynamically unstable that any mesopores present would immediately collapse upon removal of the mesopore template. In this study we show that meso-$HSiO_{1.5}$ can be synthesized by template-directed self-assembly of $HSi(OEt)_3$ under aqueous acid-catalyzed conditions and after template extraction remains stable to 300 °C. Above this temperature, bond redistribution reactions initiate a metamorphic transformation which eventually yields periodic mesoporous nanocrystalline silicon-silica, meso-ncSi/SiO_2, a nanocomposite material in which brightly photoluminescent silicon nanocrystallites are embedded within a silica matrix throughout the mesostructure. The integration of the properties of silicon nanocrystallinity with silica mesoporosity provides a wealth of new opportunities for emerging nanotechnologies.

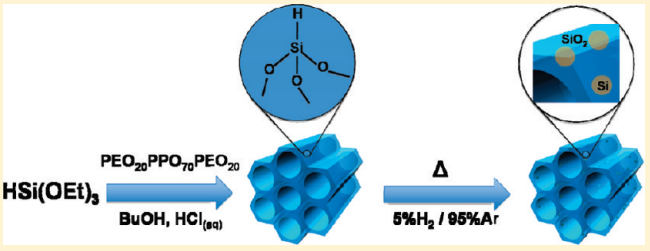

INTRODUCTION

There are innumerable examples of molecules and materials that have been targeted as realistic synthetic goals but have never been prepared due to their instability under ambient conditions. Some classic examples that do not contravene theories of valence and bonding yet remain elusive include N_6, NF_5, O_8, PH_5, and SiO_3^{2-} which are isovalent and isostructural with known molecular analogues C_6H_6, PF_5, S_8, PF_5, and CO_3^{2-}, respectively.[1] In contrast, other compounds once considered to be "impossible" have been discovered, including the inert gases that were thought too stable to participate in bonding with other elements and now exist as a growing family of noble gas compounds.[2] More recently, the perception of small molecules such as N_2, H_2, CH_4, and CO_2 as noncoordinating has been invalidated by myriad examples of transition metal coordination compounds incorporating these small molecules as ligands,[3−6] the instability of cyclobutadiene C_4H_4 was overcome by complexing it with appropriate organometallics,[7] the synthesis of discrete $R_2Si{=}SiR_2$ molecules containing a silicon−silicon double bond was achieved using sterically demanding organic groups on silicon for stability,[8] the utilization of the inherently unstable multiply

Received: December 21, 2010
Published: March 15, 2011

bonded P_2 molecular analogue of N_2 as a ligand in organometallic chemistry required an appropriate precursor,[9] and the long thought instability of single sheet graphene now accessible through chemical and physical methods not only turned out to be wrong but also garnered the most recent Nobel Prize.[10]

Considering "impossible" solids, it had long been thought that thermodynamics dictates the close packing of atoms in the lattice of crystals. However, the discovery of large families of naturally occurring and synthetic zeolites with massive internal void spaces quickly overturned that belief[11] and established that kinetic stability dominates over thermodynamic stability in these types of metastable open framework solids.[12] Over half a century of research on template-directed synthesis of zeolites had created the impression that obtaining pore sizes beyond the microporous limit of 2 nm would be impossible. However, this also proved to be wrong with the discovery that periodic mesoporous silicas (PMS) with pore sizes in the 2−50 nm range could be synthesized with supramolecular templates comprised of surfactant or block copolymer assemblies.[13−15] In this context, a prevailing opinion in the field of zeolites and PMS is that the stability of these solids with respect to densification is predicated upon the existence of a robust four-connected network of tetrahedral SiO_4 building blocks and that a maximum of 25% three-connected $RSiO_3$ units, where R is a hydroxyl or a terminal organic group, can be tolerated before the open-framework collapses.[16] This represents the current opinion regarding the stability of connected compared to disrupted periodic micro- and mesoporous silicas. From this extensive experience and these established principles, periodic mesoporous hydridosilica (meso-$HSiO_{1.5}$) should not exist because it would have a structure based on an inherently unstable fully disrupted silica framework comprised of a three-connected three-dimensional network of tetrahedral $HSiO_3$ building blocks, which would tend to collapse to dense $HSiO_{1.5}$.

In the work described herein we demonstrate that meso-$HSiO_{1.5}$ can be synthesized through aqueous acid-catalyzed template-directed self-assembly of $HSi(OEt)_3$, and after template extraction the mesopore structure remains intact up to temperatures of 300 °C. Furthermore, in the higher temperature range of 300−1000 °C, rather than exhibiting densification, meso-$HSiO_{1.5}$ instead undergoes a unique metamorphic transformation in which the hydridosilicate pore walls undergo disproportionation reactions without collapse into brightly photoluminescent nanocrystalline silicon embedded within a silica matrix. This novel nanocomposite, denoted meso-ncSi/SiO_2, in which the periodic mesoporous structure is preserved, offers control over the size and photoluminescence of silicon nanocrystals through variations to the thermal treatment. The ability to organize luminescent silicon nanocrystals within a high surface area periodic mesoporous material bodes well for the development of light emitting, solar energy, and biological sensor devices.

EXPERIMENTAL SECTION

Synthesis of Periodic Mesoporous Hydridosilica (meso-$HSiO_{1.5}$). In a typical synthesis, 1.68 g of Pluronic-123 surfactant (P123 triblock copolymer, BASF Corporation) and 3.0 g of NaCl were dissolved in 60 mL of $HCl_{(aq)}$ (0.1 M) with rapid mechanical stirring at room temperature. After complete dissolution of both components, 1.2 mL of *n*-butanol (99.9%, ACP) was added to the solution. The role of NaCl is to define the micellar structure and enhance the micellization of the P123. Butanol is inserted into the hydrophilic−hydrophobic interface of the P123 micelles, adjusting the interface curvature in order to obtain optimum meso-ordering. After 1 h of continuous stirring, 4.5 mL of triethoxysilane ($HSi(OEt)_3$) (95%, Aldrich) was rapidly added to the homogeneous and clear aqueous solution. The synthesis was carried out in acidic conditions not only to ensure proper hydrolysis and condensation rates but also to minimize hydrolysis of the Si−H bond, which is essential for the subsequent formation of SiO_2-embedded ncSi. The mixture was constantly stirred at room temperature for 12 h, and the resulting white product precipitate was isolated by centrifugation. The surfactant was subsequently removed through Soxhlet extraction over ethanol/HCl for 24 h, and the solid was finally washed with 0.1 M $HCl_{(aq)}$. The resulting white power was dried *in vacuo* at 60 °C for 12 h and stored *in vacuo* prior to use to minimize hydrolysis and oxidation.

Thermal Processing of meso-$HSiO_{1.5}$ and Formation of Periodic Mesoporous Nanocrystalline Silicon-Silica Composite (meso-ncSi/SiO_2). Solid meso-$HSiO_{1.5}$ was placed in a quartz reaction boat and transferred to a high temperature tube furnace. Samples were heated to defined peak processing temperatures (300−1100 °C) at 20 °C/min in a slightly reducing atmosphere (5% H_2/95% Ar), and the temperature was maintained for 1 h. After cooling to room temperature, solids ranging in color from white to dark amber were obtained.

Materials Characterization. Solid-state NMR was performed on a Bruker Avance 200 MHz spectrometer using a 7 mm zirconia rotor and magic-angle spinning (MAS) at a spinning frequency of 5000 Hz. The ^{29}Si high-power decoupling (HPDEC) MAS NMR measurement was performed with a 5 μs 90° pulse, a 30 s recycle delay, and a 5 μs prescan delay. The ^{13}C cross-polarized (CP) MAS experiment was performed with a 10 ms contact time using composite pulse proton decoupling. Fourier Transform Infrared (FTIR) spectroscopy was performed on a Perkin-Elmer Spectrum One FTIR spectrometer. Solid samples were mixed with KBr, ball milled into a fine powder, and pressed into a dense pellet for analysis. Raman spectroscopy was performed using a 532 nm diode laser and calibrated using a crystalline silicon wafer. Powder X-ray diffraction (PXRD) patterns of all samples were obtained on low intensity background substrates and acquired using a Siemens D5000 using Cu K_α radiation (λ = 0.15418 nm) and a SAXS Nanostar Small Angle X-ray Scattering diffractometer equipped with high-power point focus Cu K_α source. SEM images were obtained by Hitachi S-5200 at 5 kV. TEM images were obtained using an image corrected FEI Titan 80−300 equipped with a Gatan US 1000 CCD camera and operated under semi low-dose conditions at 80 kV (powder samples) and 300 kV (FIB prepared TEM lamella). TEM samples were prepared by spreading the dry powder on carbon coated copper grids (Quantifoil R2/1) or by in situ lift-out using a FEI Strata 400S operated at 5 kV for the final polishing of the TEM lamella. Sorption experiments were performed by a Quantachrome Autosorb-1C machine with N_2 as sorption gas at 77 K starting at a relative pressure $P/P_0 = 10^{-5}$. Seven data points were selected for BET analysis from a P/P_0 of 0.1. XPS were acquired using a Thermo Scientific Theta Probe utilizing monochromatic Al K_α radiation. UV−vis absorption spectra were recorded on a Perkin-Elmer Lambda 900 UV−vis-NIR spectrometer. Samples were mounted between two quartz substrates, and absorption spectra were recorded using a diffuse reflectance attachment and collected between 200 and 1000 nm with a scan speed of 70 nm/min. Photoluminescence spectra were evaluated at room temperature using the 325 nm line of a He−Cd laser excitation source, and emission was detected with a fiber-optic digital charge-coupled device (CCD) spectrometer whose spectral response was normalized using a standard blackbody radiator.

RESULTS AND DISCUSSION

We present the synthesis of periodic mesoporous hydridosilica (meso-$HSiO_{1.5}$) through the template-directed self-assembly of $HSi(OEt)_3$, and its thermally induced transformation into periodic mesoporous nanocrystalline silicon-silica (meso-ncSi/SiO_2)

dx.doi.org/10.1021/ja111495x | J. Am. Chem. Soc. 2011, 133, 5094–5102

Scheme 1. Synthesis of meso-$HSiO_{1.5}$ from the Templated Hydrolysis and Condensation of Triethoxysilane, $HSi(OEt)_3$, and Its Transformation into meso-ncSi/SiO_2 by Heating in a Slightly Reducing 5% H_2/95% Ar Atmosphere

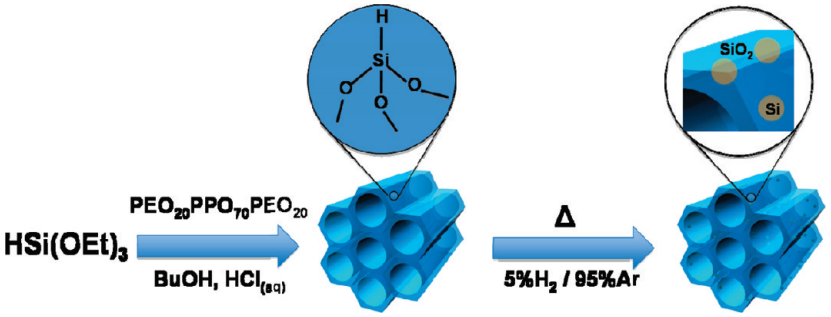

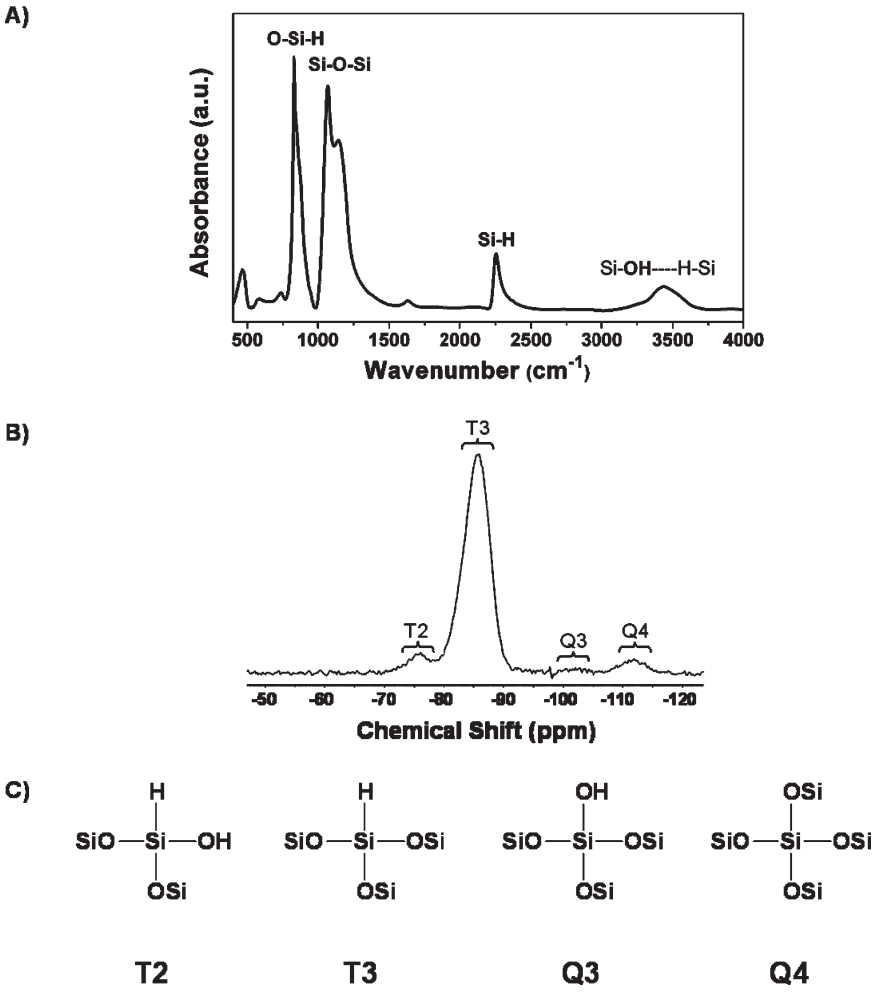

Figure 1. Compositional characterization of meso-$HSiO_{1.5}$. **A**) FTIR spectrum showing characteristic Si−H, Si−O−Si, and H−Si−O stretching modes from $HSiO_{1.5}$ and residual Si−OH from uncondensed silanol groups. **B**) ^{29}Si HPDEC MAS NMR spectrum resolved into component T2, T3, Q3, and Q4 centers. **C**) Schematic representation of T and Q centers comprising the meso-$HSiO_{1.5}$.

composite (Scheme 1). Of particular note, meso-$HSiO_{1.5}$, with pore walls composed primarily of $HSiO_3$ tetrahedral building units, represents a rare example of a fully interrupted framework material with a novel mesopore wall structure and composition. Furthermore, as bulk $HSiO_{1.5}$ materials are known to be precursors for the thermally driven formation of SiO_2-embedded ncSi,[17−19] we demonstrate that these same chemical transformations occur within the pore walls of meso-$HSiO_{1.5}$, thereby generating luminescent meso-ncSi/SiO_2 with ncSi embedded throughout the mesostructure.

Periodic Mesoporous Hydridosilica (meso-$HSiO_{1.5}$). The composition of the meso-$HSiO_{1.5}$ was confirmed by FTIR and Raman spectroscopy and ^{29}Si HPDEC MAS NMR. The FTIR spectrum (Figure 1A) shows a sharp Si−H stretching vibration at

dx.doi.org/10.1021/ja111495x |*J. Am. Chem. Soc.* 2011, 133, 5094–5102

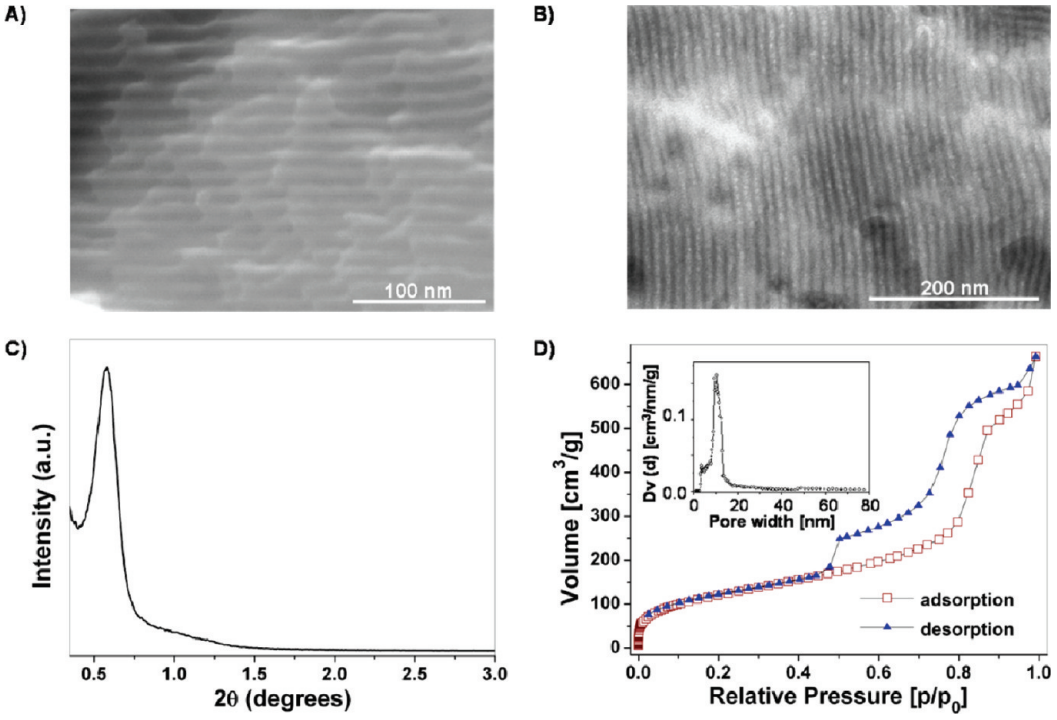

Figure 2. Structural characterizations of meso-$HSiO_{1.5}$. **A**) SEM image, **B**) TEM image, **C**) SAXS diffraction pattern, and **D**) N_2 adsorption−desorption isotherms and DFT pore size distribution (inset) of meso-$HSiO_{1.5}$.

ca. 2255 cm^{-1}, an intense Si−O−Si vibration at 1000−1300 cm^{-1}, and a H−Si−O hybrid vibration at 800−900 cm^{-1}, consistent with an empirical composition of $HSiO_{1.5}$.[17] The relatively broad peak at ca. 3500 cm^{-1} is attributed to Si−OH groups, originating either from hydrolyzed Si-OEt groups or to limited hydrolysis of Si−H bonds. The shift, broadening, and structure of the peak at 3500 cm^{-1} is an indication of hydrogen bonding between the Si−OH sites, likely with other silanols, water, or Si−H sites in the framework.[20] The FTIR and Raman spectra also show very little residual carbon from unhydrolyzed Si-OEt groups or residual surfactant, also supported by the ^{13}C CP MAS NMR spectrum (Supporting Information Figure S1). Similar FTIR spectra have been reported for cage-like hydrogen silsesquioxane (HSQ) and other dense $(HSiO_{1.5})_n$ extended network (ladder or random) structures.[17,21,22] Considering the Si−O−Si stretching and H−Si−O deformation bands (Figure 1A), previous studies have shown that their intensities and frequencies are related to the structure of the $HSiO_{1.5}$ framework, with the high frequency component of these bands (ca. 1160 cm^{-1} for Si−O−Si and ca. 875 cm^{-1} for H−Si−O) as vibrations of the cage-like structure of HSQ, while the lower frequency components (ca. 1075 cm^{-1} for Si−O−Si and ca. 830 cm^{-1} for H−Si−O) as vibrations of a ladder network structure.[23,24] Furthermore, the peak at 465 cm^{-1} has also been associated with cage-like structures.[21,22] Therefore, it can be concluded that the pore walls in the meso-$HSiO_{1.5}$ are composed primarily of mixed ladder network and cage-like $HSiO_{1.5}$ structures. The Raman spectra of the as-synthesized and surfactant-extracted samples (Supporting Information Figure S2) show that there is a weak interaction between the surfactant molecules and the $HSiO_{1.5}$ walls, causing broadening and a small shift of the H−Si mode at ca. 2265 cm^{-1}, supporting the above proposal.

Further insight into the composition of the meso-$HSiO_{1.5}$ was obtained from ^{29}Si HPDEC MAS NMR (Figure 1B). The spectrum shows four peaks at −75.7, −86.0, −102.2, and −111.6 ppm, which can be assigned to various T and Q Si centers (Figure 1C).[25] Quantification of each component yielded a composition of 7.6% T_2 $HSi(OSi)_2(OH)$, 85.3% T_3 $HSi(OSi)_3$, 1.8% Q_3 $(OH)Si(OSi)_3$, and 5.2% Q_4 $Si(OSi)_4$, indicating that the meso-$HSiO_{1.5}$ is composed primarily of $HSiO_{1.5}$ (T) centers. A small amount of SiO_2 (Q) centers is due to slight hydrolysis of Si−H bonds. The T3 peak has two components, one at −84.7 ppm (50.9%, relatively broad with a fwhm of 5.6 ppm) and the other at −86.3 ppm (34.4%, sharper with a fwhm of 3.9 ppm), likely due to ladder and cage $HSiO_{1.5}$ species, respectively.

Further structural information on the meso-$HSiO_{1.5}$ was obtained by direct imaging of the mesostructure by electron microscopy. Interestingly, under the present synthetic conditions, meso-$HSiO_{1.5}$ predominantly adopts a spherical particle morphology (*vide infra*), with diameters ranging from 100−400 nm (Supporting Information Figure S3). Both SEM and TEM images show the presence and periodic parallel alignment of mesoporous channels (Figure 2A, B), although the pore ordering becomes somewhat disordered for the smallest spherical particles. The TEM images display an approximate pore−pore distance of ∼14 nm, a pore diameter of ∼8 nm, and a wall thickness of ∼6 nm. The long-range ordering of the mesoporous structure was also verified by small-angle X-ray scattering (SAXS) (Figure 2C). The intense (100) diffraction line at 0.58°, 2θ, corresponds to a d-spacing of 15.2 nm (approximate unit cell parameter a = 17.6 nm) and unresolved (110) and (200) lines at ca. 1.00 and 1.16°, 2θ, respectively, are indicative of a regular arrangement of 2D hexagonal mesopores. Additionally, N_2 sorption data give clear evidence of the mesoporosity of the meso-$HSiO_{1.5}$ (Figure 2D). The adsorption−desorption branches display type IV isotherms, typical for mesoporous materials,[26] with a BET surface area of 434 m^2/g and a narrow pore size distribution centered at 10.5 nm

dx.doi.org/10.1021/ja111495x | *J. Am. Chem. Soc.* 2011, 133, 5094–5102

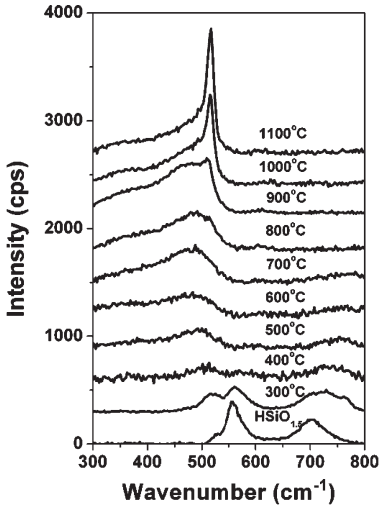

Figure 3. Thermal transformation of meso-$HSiO_{1.5}$ to meso-ncSi/SiO_2. Evolution of the Raman spectrum of meso-$HSiO_{1.5}$ as a function of heating from 300 to 1100 °C under a slightly reducing atmosphere (5%H_2/95% Ar).

(Figure 2D, inset). The observed hysteresis occurs as a result of capillary condensation in mesopores with diameters larger than ca. 4 nm. The shape of the isotherm, classified as Type IV, for meso-$HSiO_{1.5}$ agrees with the TEM images, which indicates that it contains ordered uniformly sized cylindrical pores. Together with the unit cell parameter obtained from the SAXS pattern and the data obtained from BET measurements, the wall thickness has been estimated to be around 7.1 nm.

Transformation of meso-$HSiO_{1.5}$ into Periodic Mesoporous Nanocrystalline Silicon-Silica Composite (meso-ncSi/SiO_2). Similar to its dense analogue $HSiO_{1.5}$, thermal treatment of meso-$HSiO_{1.5}$ in a slightly reducing atmosphere (5% H_2/95% Ar) leads to thermally induced rearrangement and disproportionation reactions, driving the diffusion of Si atoms throughout the oxide matrix and ultimately leading to a nucleation, growth, and crystallization of silicon nanocrystals throughout the mesostructure.[17−19] The conversion of meso-$HSiO_{1.5}$ to meso-ncSi/SiO_2 as a function of thermal processing temperature is clearly demonstrated by the evolution of the Raman peak at 515 cm^{-1}, corresponding to the transverse optical phonon (TOP) mode of ncSi (Figure 3). In the spectral range 300−800 cm^{-1}, the Raman spectrum of meso-$HSiO_{1.5}$ is characterized by broad peaks centered at ca. 560 cm^{-1} and 705 cm^{-1}, attributed to Si−O−Si bending and likely symmetric H−Si−O waging modes, respectively. As the processing temperature is increased to 400 °C, the Raman peaks gradually give way to a rather featureless broad band attributed to thermally initiated rearrangement and disproportionation reactions in the hydridosilicate network. Further increasing the processing temperature results in the emergence and gradual increase in intensity of a broad peak centered at 480 cm^{-1}, characteristic of amorphous Si.[27] As the temperature is further raised from 800 to 1100 °C, the amorphous Si peak is gradually replaced by a sharp asymmetric peak at ca. 515 cm^{-1}, corresponding to the TOP mode in nanocrystalline Si.[28] The shift of the TOP to higher frequencies with increasing temperature results from phonon confinement effects and is indicative of the growth of the nanocrystalline Si domains.[28] From the peak position of the TOP for samples processed at 1100 °C,[29] an approximate diameter of ca. 3.4 nm was obtained, in agreement with Scherrer analysis of PXRD peak broadening.

The transformation of meso-$HSiO_{1.5}$ to meso-ncSi/SiO_2 is also evident from the changes in the FTIR spectra, powder X-ray diffraction (PXRD), and X-ray photoelectron spectra (XPS). The evolution of the FTIR spectra with increasing processing temperature (Supporting Information Figure S4A) shows a gradual decrease in Si−H stretching and H−Si−O vibrations, consistent with the Si−H thermolysis in the meso-$HSiO_{1.5}$. Detailed examination of the 800−1000 cm^{-1} spectral range in the FTIR spectrum (Supporting Information Figure S4B,C) provides additional insight into the initial stages of the redistribution process. At 300 °C, the low energy peaks (ca. 830 and 855 cm^{-1}), originating from the extended network of $HSiO_{1.5}$, gradually disappear, while peaks for H_2Si- and H_3Si- sites appear (906, 945, and 980 cm^{-1} and a shoulder at ca. 2200 cm^{-1}). In addition, the cage-like species (with a peak at 881 cm^{-1}) start decomposing at around 500 °C. These thermally induced transformations of the meso-$HSiO_{1.5}$ to meso-ncSi/SiO_2 are very similar to previous reports on dense forms of $HSiO_{1.5}$.[19] The PXRD patterns (Supporting Information Figure S5) show broad reflections, indexed to the (111), (220), and (311) crystal planes of the diamond structure of Si emerging for samples processed at 900 °C, along with a broad feature characteristic of the amorphous SiO_2 matrix.[18] Further increasing the temperature to 1000 and 1100 °C leads to a gradual narrowing of the diffraction peaks and an increase in their intensity, consistent with nanocrystal Si growth within the SiO_2 phase.[19] The Scherrer analysis of the XRD line broadening for the sample processed at 1100 °C gave an approximate ncSi average diameter of 3 nm. The Si 2p high resolution XPS (Supporting Information Figure S6) show typical trends for ncSi/SiO_2 composite materials,[19] consisting primarily of two spectral regions corresponding to Si(IV) and Si(0) that are separated by a nonzero baseline. At lower processing temperatures (300−400 °C), the samples are composed primarily of Si(IV) and Si(III) in the oxide network. As the processing temperature is increased, Si clustering and nanocrystal formation leads to the emergence of a low energy shoulder corresponding to Si(0), which shifts and increases in intensity as the temperature is further increased. The nonzero baseline separating the Si(IV) and Si(0) is attributed to the SiO_x interface between the Si nanocrystals and the SiO_2-like matrix.

During the thermal processing of meso-$HSiO_{1.5}$ and its transformation to ncSi/SiO_2, the periodic mesoporous structure is maintained. The SAXS data, SEM and TEM images (Figures 4 and 5) show a high degree of mesostructure ordering in materials processed at temperatures below 1000 °C, with structural collapse beginning above 1000 °C. The mesopore *d*-spacing, pore size, pore volume, wall thickness, and surface area at various stages in the transformation to meso-ncSi/SiO_2 are listed in Table 1. It can be seen that both the pore volume and surface area decrease with increasing annealing temperature and that the pore diameter also decreases without notable changes to the wall thickness. The significant decrease in surface area and pore volume at 500 °C is likely attributed to the collapse of micropores in the walls and to limited partial collapse of the mesopores at higher temperatures. The FTIR spectra of meso-$HSiO_{1.5}$ identified a significant structural contribution from cage-like domains (*vide infra*), which have been shown to collapse at $T > 450$ °C.[24] Given their large contribution to the overall surface area of the material, the observed decrease in surface area and volume are understandable. The microporosity is directly observed in the N_2 sorption isotherms of meso-$HSiO_{1.5}$ but disappears in the samples after thermal treatment at 500 °C and above (Supporting Information

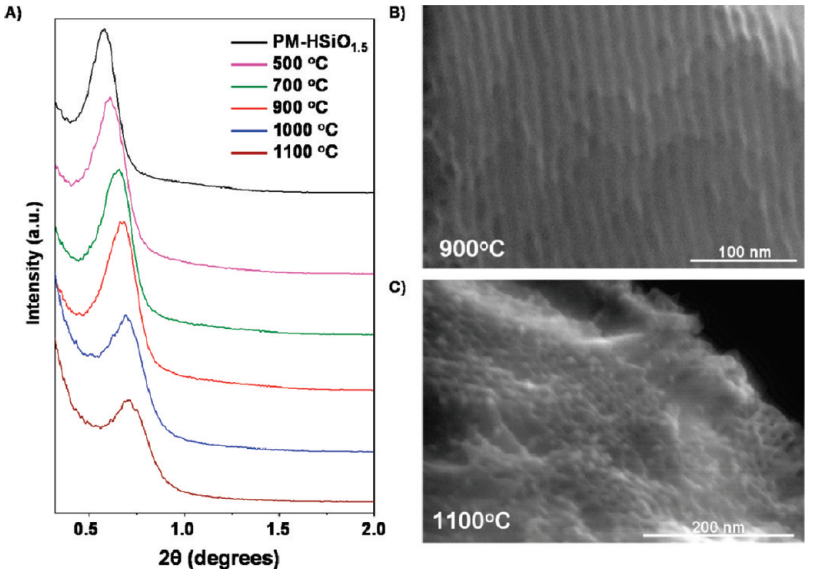

Figure 4. Structural characterizations of meso-ncSi/SiO_2. **A**) Evolution of SAXS pattern as a function of processing temperature. The SEM images after processing at **B**) 900 °C and **C**) 1100 °C.

Figure S7). Therefore, the transformation during the thermal treatment makes the walls more compact and decreases the surface area and pore volume.

The structure of meso-ncSi/SiO_2 was examined by high-resolution transmission electron microscopy (HRTEM) (Figure 5), and similar to meso-$HSiO_{1.5}$, samples processed at 900 °C (Figure 5A, C) and 1000 °C (Figure 5B, D) maintain a spherical morphology with diameters of 100−400 nm. It can be seen that a mesoporous structure remains after processing at these high temperatures, and in addition ncSi are visible on the external surface of the particles, with characteristic lattice spacings of 0.28 and 0.31 nm in agreement with crystalline silicon. Given that the formation and growth process of ncSi within a SiO_2 matrix is diffusion driven, it is not unexpected to observe nanocrystals on the external surface of the particles. In order to verify whether ncSi nucleate and grow within the pore walls of the mesostructure, a focused-ion beam (FIB) was used to obtain thin cross sections of spheres for HRTEM imaging. Figure 5E shows a cross-section of meso-ncSi/SiO_2 processed at 1000 °C, showing lattice fringes of ncSi. The ncSi are observed everywhere throughout the cross-section, indicating that the ncSi are not only located on the external surface of meso-ncSi/SiO_2 spheres but are well distributed within the spheres. From these images, it is clear that the ncSi pervade the mesostructure; however, it should be noted that it is not yet possible to distinguish between channel-embedded and pore wall-embedded ncSi.

The room temperature UV−vis absorption and photoluminescence (PL) spectra of meso-ncSi/SiO_2 are shown in Figure 6. The absorption spectra for both samples show broad absorption bands, peaking at ca. 350 nm. Fitting the absorption spectra to direct and indirect relations give a direct band gap of ca. 2.35 eV and indirect band gap of ca. 1.80 eV, consistent with the quantum confinement effect and observed PL. For samples processed at 900 °C, an intense PL peak is observed centered at ca. 690 nm. Further processing to 1000 °C leads to a shift in the PL peak to 720 nm. Given the growth of ncSi over this temperature range determined by PXRD and Raman measurements, this PL behavior is consistent with quantum confinement and size-dependent PL from the ncSi component of the nanocomposite meso-ncSi/SiO_2.[19] Although the source of PL in ncSi/SiO_2 composites has been controversial, recent X-ray Excited Optical Luminescence (XEOL) measurements on similar samples have conclusively identified quantum confinement in the ncSi core as the emission source.[30] We are currently extending this investigation to include detailed photophysical measurements to gain further insight into the origin of this luminescence.

Why Does Meso-$HSiO_{1.5}$ Exist? As previously mentioned, the synthesis of meso-$HSiO_{1.5}$ with >90% H-SiO_3 T centers is unique in the field of periodic mesoporous materials chemistry. Extensive reports on periodic mesoporous organosilicas (PMOs) have consistently pointed out that the incorporation of >25% $RSiO_3$ units leads either to the collapse of the mesoporous framework or to disordered mesostructures.[16] In these interrupted framework materials, a significant amount of SiO_4 "mortar" is required to ensure overall structural integrity and meso-ordering.

The existence of a more or less fully interrupted framework in meso-$HSiO_{1.5}$ appears to be attributed to a combination of steric and hydrogen-bonding effects. The presence of ladder units and their terminated silanol sites ensures the assembly of $HSiO_{1.5}$ species into meso-$HSiO_{1.5}$. Furthermore, the small size of the Si−H unit likely increases the overall cross-linking density in the pore walls, enabling sufficient siloxane bonds to form to withstand the stresses of template removal. This steric consideration is supported by a recent report of >50% Si-CH_3 incorporation in a terminal methyl-PMO.[31] The smaller size of Si−H relative to Si-CH_3 in the present system allows this effect to an even greater extent. Further structural support comes from the hydridic nature of Si−H, allowing hydrogen-bonding with proximal Si−OH groups (Si−H•••HO-Si) within the pore walls, as suggested in the FTIR spectra (*vide supra*). This effectively converts a nominally three-connected three-dimensional unstable silica framework into a four-connected three-dimensional stable one. Similar hydride-silanol interactions have previously been reported to be associated with the anchoring of Si_2H_6 gaseous molecules within zeolite pores and mesoporous silica.[20] In contrast, terminal organic groups in meso-$RSiO_{1.5}$ cannot

dx.doi.org/10.1021/ja111495x | *J. Am. Chem. Soc.* 2011, 133, 5094–5102

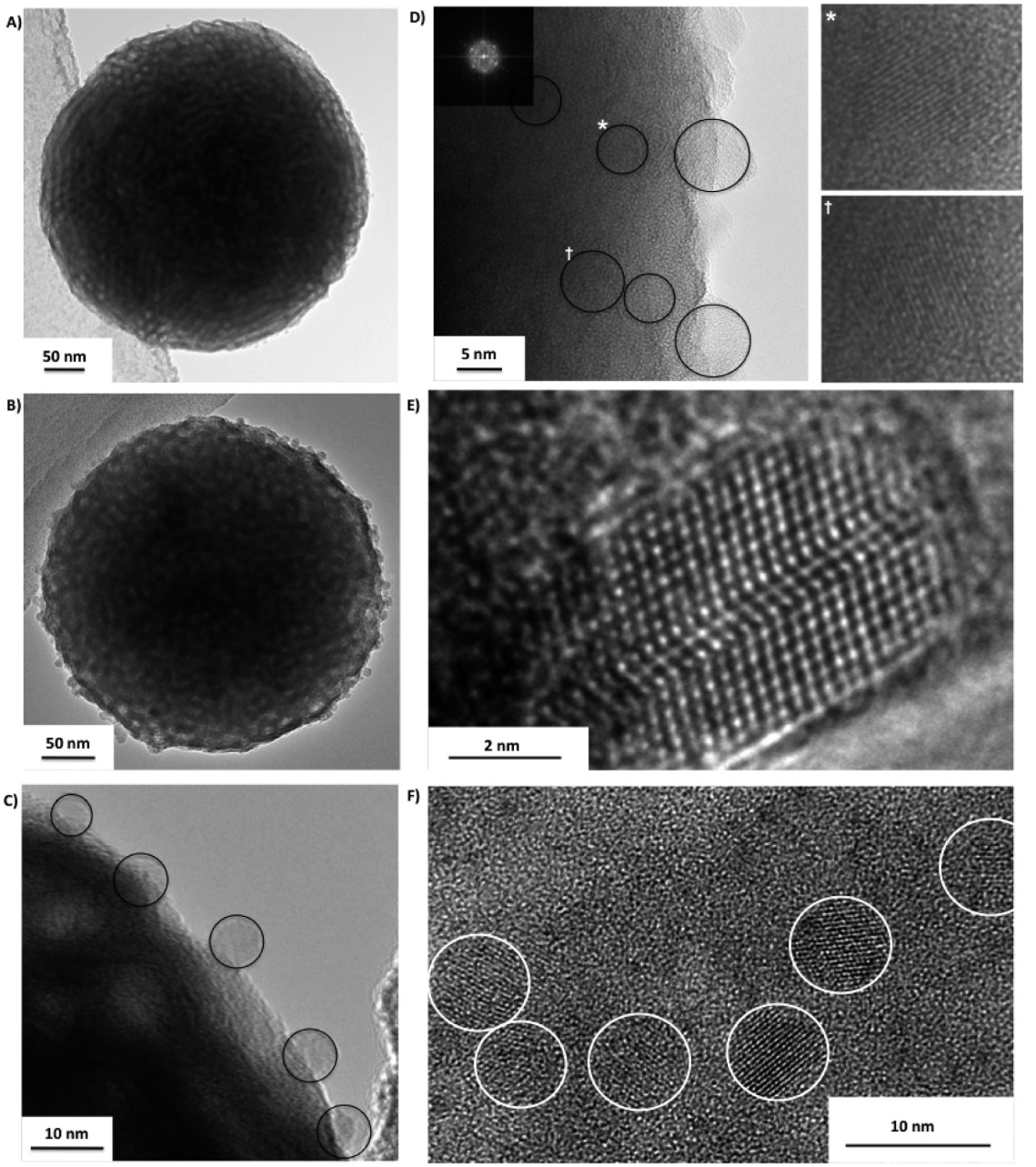

Figure 5. Structural characterizations of meso-ncSi/SiO_2. HRTEM imaging of meso-ncSi/SiO_2 processed at 900 °C (**A, C**) and 1000 °C (**B, D, E**) showing spherical morphology meso-ncSi/SiO_2 particles with mesopores and ncSi. Focused-ion beam prepared cross sections (**F**) reveal ncSi with lattice fringes of 0.31 nm throughout the spherical mesoporous particles. The additional dark spots are due to ca. 1 nm Ga droplets from the FIB processing.

participate in this stabilizing hydrogen bonding and instead have stronger interactions with the organic template. As a result, they are more likely to occupy surface sites in the pores, and if they are buried within the pore walls they disrupt the structural stability of the local environment. Because the Si—H sites can form weak hydrogen-bonding interactions with the neighboring Si—OH moieties, an increased local stability is achieved and the overall framework, even though almost completely interrupted, is stable enough to survive template removal and retain its mesoporous structure.

Why Does Meso-$HSiO_{1.5}$ Adopt a Spherical Morphology?

The hydrolysis of silicon alkoxides under acidic conditions occurs through the protonation of alkoxy groups, and is the rate determining step in the overall hydrolysis/condensation reaction. Therefore the hydrolysis step is crucial for controlling the

Table 1. Surface Area, Pore Volume, d-Spacing, Pore Diameter, and Wall Thickness at Various Stages in the Transformation from meso-$HSiO_{1.5}$ to meso-ncSi/SiO_2

sample	surface area (m^2/g)	pore volume (mL/g)	$d_{(100)}$ (nm)	pore diameter (nm)	wall thickness (nm)
PM-$HSiO_{1.5}$	434.3	0.98	15.2	10.5	7.1
500 °C	177.5	0.51	14.5	9.4	7.3
700 °C	132.4	0.38	13.4	9.1	6.4
900 °C	127.1	0.36	13.3	8.2	7.2

dx.doi.org/10.1021/ja111495x |*J. Am. Chem. Soc.* 2011, 133, 5094–5102

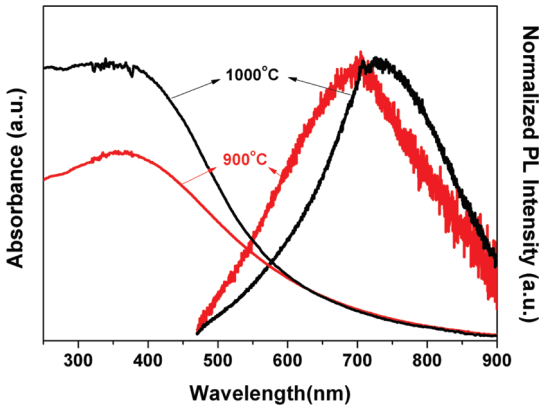

Figure 6. Optical properties of meso-ncSi/SiO_2. PL and absorption spectra for meso-$HSiO_{1.5}$ processed at 900 and 1000 °C showing intense size-dependent emission at room temperature, consistent with quantum confinement in ncSi. The absorption spectra are vertically shifted for clarity.

morphology of templated forms of mesoporous silica. The hydrogen in $HSi(OEt)_3$ is hydridic, with less electron withdrawing ability compared to the alkoxy groups in TEOS. Therefore, under acidic conditions the alkoxides of $HSi(OEt)_3$ are more susceptible to protonation and faster hydrolysis than TEOS.[16,32] As a result, the fast hydrolysis of $HSi(OEt)_3$ favors rapid formation and growth of a very large population of spherical meso-$HSiO_{1.5}$ seeds. Since molecular $HSi(OEt)_3$ feedstock is consumed so rapidly, these seeds predominantly end up as meso-$HSiO_{1.5}$ nanospheres. Additionally, it is known that spherical morphologies are favored if the pH of the templated synthesis is close to the isoelectric point of silica (~2).[33] In this context, the SEM and TEM images of meso-$HSiO_{1.5}$ display a large number of spherical mesoporous particles, supporting the above proposal. In this manner, controlling the pH of the synthesis solution around 2 yields a particle size distribution for meso-$HSiO_{1.5}$ of ca. 100−400 nm (Supporting Information Figure S3).

How Does ncSi Grow in Meso-$HSiO_{1.5}$? It is interesting to consider the effect of spatial confinement of the pore walls of meso-$HSiO_{1.5}$ on the formation and growth of ncSi within the physical limits of the pore walls. As previously mentioned, the use of $HSiO_{1.5}$ glasses, as well as other SiO_x systems, as precursors for the formation of SiO_2-embedded ncSi is well-known.[17−19] In these systems, ncSi size-control is usually achieved by changing the SiO_x composition and peak thermal processing temperature.[19,34] In SiO_x/SiO_2 superlattices, an additional size control strategy has been developed, involving the spatially confined growth of ncSi within the SiO_x layers.[35] Using controlled evaporation deposition techniques, it was found that the size of ncSi was dependent on SiO_x layer thicknesses ranging from 2 to 7 nm, with thicker layers giving rise to larger ncSi.[35] Considering that the pore wall thickness of meso-$HSiO_{1.5}$ is 7 nm, it is possible that similar growth constraints affect the growth of ncSi. Compared to bulk $HSiO_{1.5}$ samples processed under identical conditions, the present ncSi are smaller (as determined by Scherrer analysis of PXRD peak broadening), and their PL is significantly more blue-shifted, consistent with smaller ncSi. These observations strongly support the role of pore wall thickness in governing the ncSi diameter during the thermal processing of meso-$HSiO_{1.5}$. This offers an interesting opportunity to explore the spatially confined growth of ncSi in pore walls of different thickness.

CONCLUSION

We present the synthesis and characterization of periodic mesoporous hydridosilica (meso-$HSiO_{1.5}$) and its thermally induced metamorphic reconstruction into photoluminescent periodic mesoporous nanocrystalline silicon-silica composite (meso-ncSi/SiO_2). Detailed characterization of the hydridosilica confirms its periodic mesoporous structure and the composition of the mesopore walls as $HSiO_{1.5}$. The existence of meso-$HSiO_{1.5}$, which would have previously been considered "impossible" because of its completely interrupted open framework structure, appears to be related to the combined benefits of SiOH•••HSi hydrogen bonding and the small steric demand of Si−H groups. Together, these effects contribute to an enhancement in the mechanical stability and resistance to collapse of the mesopores upon removing the template and subsequent thermal treatment to around 300 °C. Thermal processing at higher temperatures in a slightly reducing atmosphere leads to disproportionation and rearrangement reactions which ultimately result in the nucleation and growth of ncSi within the pore walls, while maintaining the periodic mesoporous structure intact. Compared to bulk materials processed under identical conditions, it was found that the spatial confinement of the pore walls constrained the growth of ncSi to smaller sizes. The resulting meso-ncSi/SiO_2 nanocomposite materials are brightly luminescent and exhibit size-controlled photoluminescence in accordance with the principles of quantum confinement.

ASSOCIATED CONTENT

Supporting Information. Further characterization of meso-$HSiO_{1.5}$ and its thermally induced transformation into meso-ncSi/SiO_2. This material is available free of charge via the Internet at http://pubs.acs.org.

AUTHOR INFORMATION

Corresponding Author

*E-mail: gozin@chem.utoronto.ca (G.A.O.), E-mail: gu@seu.edu.cn (Z.-Z.G.).

ACKNOWLEDGMENT

G. A. Ozin is the Government of Canada Research Chair in Materials Chemistry and Nanochemistry. He thanks the Natural Sciences and Engineering Research Council (NSERC) of Canada for strong and sustained financial support of his research. Ö. Dag thanks Bilkent University and Turkish Academy of Science for financial support. I. Moudrakovski and the Steacie Institute for Molecular Sciences at the National Research Council of Canada are thanked for assistance with solid state NMR, A. Reijnders and K. Burch for assistance with Raman spectroscopy, S. Petrov for XRD measurements, and J. Kelly and J. Veinot for assistance with PL spectroscopy.

REFERENCES

(1) Dasent, W. E. *J. Chem. Educ.* **1963**, *40*, 130.
(2) Grochala, W. *Chem. Soc. Rev.* **2007**, *36*, 1632.
(3) Fryzuk, M. D. *Chem. Rec.* **2003**, *3*, 2.
(4) Kubas, G. J. *Proc. Natl. Acad. Sci.* **2007**, *104*, 6901.
(5) Shilov, A. E.; Shulpin, G. B. *Chem. Rev.* **1997**, *97*, 2879.
(6) Yin, X.; Moss, J. R. *Coord. Chem. Rev.* **1999**, *181*, 27.

(7) Emerson, G. F.; Watts, L.; Pettit, R. *J. Am. Chem. Soc.* **1965**, *87*, 131.
(8) West, R. *Pure Appl. Chem.* **1983**, *56*, 163.
(9) Piro, N. A.; Figueroa, J. S.; McKellar, J. T.; Cummins, C. C. *Science* **2006**, *313*, 1276.
(10) Nobel Prize, 2010.
(11) Davis, M. E.; Lobo, R. F. *Chem. Mater.* **1992**, *4*, 756.
(12) Cheetham, A. K.; Forey, G.; Loiseau, T. *Angew. Chem., Int. Ed.* **1999**, *38*, 3269.
(13) Beck, J. S.; Vartuli, J. C.; Roth, W. J.; Leonowicz, M. E.; Kresge, C. T.; Schmitt, K. D.; Chu, C. T. W.; Olson, D. H.; Sheppard, E. W.; McCullen, S. B.; Higgins, J. B.; Schlenker, J. L. *J. Am. Chem. Soc.* **1992**, *114*, 10834.
(14) Kresge, C. T.; Leonowicz, M. E.; Roth, W. J.; Vartuli, J. C.; Beck, J. S. *Nature* **1992**, *359*, 710.
(15) Zhao, D.; Feng, J.; Huo, Q.; Melosh, N.; Fredrickson, G. H.; Chmelka, B. F.; Stucky, G. D. *Science* **1998**, *279*, 548.
(16) Wang, W.; Lofgreen, J. E.; Ozin, G. A. *Small* **2010**, *6*, 2634.
(17) Henderson, E. J.; Kelly, J. A.; Veinot, J. G. C. *Chem. Mater.* **2009**, *21*, 5426.
(18) Hessel, C. M.; Henderson, E. J.; Veinot, J. G. C. *Chem. Mater.* **2006**, *18*, 6139.
(19) Hessel, C. M.; Henderson, E. J.; Veinot, J. G. C. *J. Phys. Chem. C* **2007**, *111*, 6956.
(20) Chomski, E.; Dag, O.; Kuperman, A.; Coombs, N.; Ozin, G. A. *Chem. Vap. Deposition* **1996**, *2*, 8.
(21) Frye, C. L.; Collins, W. T. *J. Am. Chem. Soc.* **1970**, *92*, 5586.
(22) Park, E. S.; Ro, H. W.; Nguyen, C. V.; Jaffe, R. L.; Yoon, D. Y. *Chem. Mater.* **2008**, *20*, 1548.
(23) Loboda, M. J.; Grove, C. M.; Schneider, R. F. *J. Electrochem. Soc.* **1998**, *145*, 2861.
(24) Yang, C. C.; Chen, W. C. *J. Mater. Chem.* **2002**, *12*, 1138.
(25) Albert, K.; Bayer, E. *J. Chromatogr.* **1991**, *544*, 345.
(26) Rouquerol, J.; Avnir, D.; Fairbridge, C. W.; Everett, D. H.; Haynes, J. H.; Pernicone, N.; Ramsay, J. D. F.; Sing, K. S. W.; Unger, K. K. *Pure Appl. Chem.* **1994**, *66*, 1739.
(27) Iqbal, Z.; Veprek, S. *J. Phys. C* **1982**, *15*, 377.
(28) Zi, J.; Bascher, H.; Falter, C.; Ludwig, W.; Zhang, K.; Xie, X. *Appl. Phys. Lett.* **1996**, *69*, 200.
(29) Yang, C. C.; Li, S. *J. Phys. Chem. B* **2008**, *112*, 14193.
(30) Hessel, C. M.; Henderson, E. J.; Kelly, J. A.; Cavell, R. G.; Sham, T.-K.; Veinot, J. G. C. *J. Phys. Chem. C* **2008**, *112*, 14247.
(31) Pai, R. A.; Watkins, J. J. *Adv. Mater.* **2006**, *18*, 241.
(32) Kanamori, K.; Nakanishi, K. *Chem. Soc. Rev.* **2011**, *40*, 754.
(33) Yang, H.; Vovk, G.; Coombs, N.; Sokolov, I.; Ozin, G. A. *J. Mater. Chem.* **1998**, *8*, 743.
(34) Meldrum, A.; Hryciw, A.; MacDonald, A. N.; Blois, C.; Marsh, K.; Wang, J.; Li, Q. *J. Vac. Sci. Technol., A* **2006**, *24*, 713.
(35) Yi, L. X.; Scholz, R.; Zacharias, M. *J. Lumin.* **2007**, *122−123*, 750.